Available online at www.sciencedirect.com

SciVerse ScienceDirect

Ceramics International 38 (2012) 5433–5443

CERAMICS INTERNATIONAL

www.elsevier.com/locate/ceramint

$LaCoO_3$ ceramics obtained from reactive powders

L. Predoana [a], B. Malic [b], D. Crisan [a], N. Dragan [a], M. Anastasescu [a], J. Calderon-Moreno [a], R. Scurtu [a,*], M. Zaharescu [a]

[a] "Ilie Murgulescu" Institute of Physical Chemistry, Romanian Academy, 202 Splaiul Independentei, 060021 Bucharest, Romania
[b] Jozef Stefan Institute, 39 Jamova, 1001 Ljubljana, Slovenia

Received 13 February 2012; received in revised form 23 March 2012; accepted 23 March 2012
Available online 11 April 2012

Abstract

The aim of the present study was to establishing the correlation between the structure and properties of the $LaCoO_3$ powders obtained by aqueous sol–gel method with citric acid and their sintering behavior in order to obtain fully densified ceramics with perovskite structure. Two types of cobalt and lanthanum reagents were used in synthesis, namely nitrates and acetates. The sintering was realized at temperatures ranging between 800 and 1200 °C for 2 h. The sintered samples were investigated by classical ceramic methods (shrinkage, density, porosity) and by structural and morphological investigations: XRD, SEM, AFM and XPS. The electrical properties of the samples were determined by impedance spectroscopy. The ceramics obtained with powders starting with acetates have presented a lower sintering ability as compared with the samples obtained from powders starting with nitrates. $LaCoO_3$ ceramics with best properties was obtained from powders starting with nitrates sintered at 1100 °C.

Keywords: A. Sintering; C. Electrical properties; Aqueous sol–gel method; $LaCoO_3$ nano-sized powders

1. Introduction

For a better control of morphology in the final product, development of ''nonconventional'' routes for the preparation of perovskite-type oxides is of high interest [1]. $LaCoO_3$-based materials have high ionic conductivity and predominant electronic conductivity. Those materials belong to the group of the most promising mixed conductors. $LaCoO_3$ exhibit interesting electrical, magnetic and catalytic properties, being used as cathode material for solid oxide fuel cells (SOFC), catalysts for light hydrocarbon oxidation and gas detection sensors [2]. For other applications as oxygen separation from air and for synthetic-gas production [3], dense ceramic membranes with well defined microstructure are required.

Most commonly the mixed oxides have been prepared, by milling-calcinations procedure, leading to low surface area, poorly active materials and elevated temperatures of calcination (7 days at 980 °C [4] and 24 h at 1200 °C, respectively [5]).

In order to overcome these disadvantages several innovative methods were developed. Kleveland et al. [3] used a chemical route starting with nitrates and ethylendiamine tetracetic acid and a consequent thermal treatment of 15 h at 950 °C, while Faaland et al. [6] applied a spray pyrolysis method starting with the same precursors and a calcination of the resulted samples for 10 h at 900 °C. Berger et al. [2] proposed a combustion method followed by thermal treatment of 3 h at 800 °C. Li et al. [5] presented a combined method of milling nitrates with nitric acid and coprecipitation of the resulted mixture with potassium hydroxide. The resulted sample was thermally treated for 2 h at 600 °C and 800 °C, respectively. Popa et al. [7,8] reported $LaCoO_3$ powders preparation from the La–Co metal polymeric precursor by means of a simple Pechini-type polymerizable complex (PC). Nanopowders of $LaCoO_3$ with crystal size of 20–25 nm and free of polycrystalline aggregates were obtained at 550 °C.

Among the wet chemical method, several sol–gel routes were applied in order to prepare $LaCoO_3$. The so-called citrate or tartrate sol–gel method, allows to obtain powders with well defined morphology, good stoichiometric control and good particle size distribution, at low temperature and short period for calcinations [9,10]. Such powders have relatively high surface area, up to two orders of magnitude higher than for the samples prepared by calcinations-milling procedure.

The sol–gel method using mixture of alkoxides and inorganic salts as starting reagents – $La(O^iPr)_3$ and $Co(NO_3)_2$

* Corresponding author. Tel.: +40 21 318 85 95; fax: +40 21 312 11 47.
E-mail addresses: rscurtu@icf.ro, rares.scurtu@gmail.com (R. Scurtu).

0272-8842/$36.00
http://dx.doi.org/10.1016/j.ceramint.2012.03.054

– was used by Hwang [11]. The polymerizable complex method was used by Guo [12], while the carboxylic route was applied by Taguchi starting with nitrate of lanthanum or cobalt and citric acid as chelating agent [10].

For reactive powders sintering Nakayama et al. [13] used shorter time of sintering but temperatures up to 1500 °C. In the same time Chang et al. [14] studied the influence of sintering atmosphere on the sintering behavior of mixed-conducting membranes based on $LaCoO_3$.

In our previous paper [15] $LaCoO_3$ powders were obtained by aqueous sol–gel method starting with lanthanum and cobalt nitrate and acetate and citric acid as chelating agent. The resulted gels were thermally treated at 600 °C for 6 h.

The aim of the present paper was to establishing the correlation between the structure and properties of the $LaCoO_3$ powders obtained by aqueous sol–gel method and their sintering behavior in order to obtain fully densified ceramics with perovskite structure.

2. Experimental procedure

The composition of the starting solutions and the experimental conditions used were described in more details in a previous paper [15]. $LaCoO_3$ perovskite samples were prepared starting from 0.25 M aqueous solutions of $La(NO_3)_3{\cdot}6H_2O$ and $Co(NO_3)_2{\cdot}6H_2O$ or $La(CH_3COO)_3$ and $Co(CH_3COO)_2{\cdot}4H_2O$ as ion metal sources and citric acid as chelating agent.

The obtained gels were thermally treated in air at 400 °C for 1 h with a heating rate of 1 °C/min and at 600 °C for 6 h with a heating rate of 5 °C/min. From the calcinated powders pallets with 10 mm diameter and height of 2 mm were made by uni-axial pressing under 80 MPa, without any binding material addition.

The sintering was realized at temperatures ranging between 800 and 1200 °C, for 2 h soaking time. The sintered samples were investigated by classical ceramic methods (shrinkage, density, porosity) and by structural and morphological investigations: XRD, SEM, AFM and XPS.

The annealed samples were evaluated by X-ray diffraction using a CuKα (λ = 0.1540 nm) radiation source in a BRUKER AXS D4 ENDEAVOR X-ray diffractometer. The diffraction angles (2θ) range between 10° and 90° was scanned.

The specific surface area (BET method) of the powders was measured by nitrogen sorption analysis at −196 °C using a Micromeritics ASAP 2020 Analyzer.

Scanning electron microscopy (SEM) was used to examine the surface morphology, with a Zeiss EVO LS10 environmental SEM microscope.

The AFM experiments were carried out in intermittent contact mode, using an EasyScan2 apparatus from Nanosurf® AG Switzerland, with a scan rate around 1–2 Hz, equipped with sharp tips (<10 nm radius, NCLR type from Nanosensors™) with spring constant around 32 N/m and vibrating frequency of about 166 kHz.

Surface analysis performed by X-ray photoelectron spectroscopy (XPS) was carried out on PHI Quantera equipment with a base pressure in the analysis chamber of 10^{-9} Torr. The X-ray source was monochromatized Al Kα radiation (1486.6 eV) and the overall energy resolution is estimated at 0.70 eV by the full width at half-maximum (FWHM) of the Au 4f7/2 photoelectron line (84 eV). Although the charging effect was minimized by using a dual beam (electrons and Ar ions) as neutralizer, the spectra were calibrated using the C 1s line (BE = 284.8 eV) of the adsorbed hydrocarbon on the sample surface (C–C or $(CH)_n$ bondings). As this spectrum was recorded at the start and the end of each experiment the energy calibration during experiments was quite reliable.

Impedance spectroscopic measurements were conducted in air in the temperature range of 27–800 °C, and over the frequency range of 1 Hz–3 MHz, amplitude of 100 mV with a Solartron 1260 FRA. The sample was placed in ProboStat A sample holder (NorECs AS) and heated up using Elite TSV12/50/300 vertical tube furnace. For a good contact with the electrodes the pellets were coated with silver paste on both surfaces and fired at 500 °C for 1 h. IS data were corrected for the geometric factor of the sample (thickness/electrode area), the stray capacitance of the sample holder and the resistance and inductance of the measuring leads by using Zview fitting software [16].

The samples obtained from nitrates were labeled N1 and the samples obtained from acetates were labeled A1.

3. Results and discussion

3.1. Powder characterization

3.1.1. Structural characterization

Starting with cobalt and lanthanum nitrates and acetates precursors and in the experimental conditions presented above, in both cases red gels were obtained.

The UV–vis results of the obtained gels (not presented here) [17] show the presence of the Co^{2+}ion, mainly in an octahedral coordination, while the FT-IR spectra underline that citric acid act as bidentate chelating agent in the case of the samples obtained starting with nitrate and as monodentate ligand, when acetates were used as metal precursors [15].

In both cases the dried gels were amorphous, as determine by XRD. Pure $LaCoO_3$, perovskite phase was formed after heat treatment at 600 °C (Fig. 1). Except the data presented by Popa et al. [7], this temperature is the lowest mentioned in the literature data, for pure $LaCoO_3$ phase formation.

The XRD evaluation of the crystallographic parameters of the thermally treated powders is presented in Table 1, together with corresponding BET surface area values.

The presented results (Table 1) have shown in both cases the rhombohedral perovskite structure of the crystals but higher particles size and higher surface area when acetates were used as precursors. This fact could be explained by the higher organic content in the acetate based precursor gel due to the type of reagents used. By thermal treatment the organic part is eliminated leaving a high porosity of the powder. By thermal treatment up to 600 °C the pores did not entirely collapse and powder with intra-granular porosity resulted.

It is expected that the mentioned differences in the powders morphology should influence their sintering ability.

3.2. Powder morphology

The SEM images of the $LaCoO_3$ powders are presented in Fig. 2. In both cases a homogeneous particle size and particle size distribution is observed. The powder obtained starting with nitrates has particles with average size about 50 nm, while starting with acetates the average particles size is about 70 nm. These values are comparable with TEM results determined on similar powders prepared before [15].

3.3. Sintered samples characterization

3.3.1. Ceramic properties

The ceramic properties of the sintered samples at temperatures ranging from 800 °C to 1200 °C, using the powders discussed above, are presented in Table 2.

One may notice that with thermal treatment the variation of the shrinkage and porosity of the samples obtained from both powders present close values. However, the ceramics obtained from the powders prepared from acetates have shown lower densities as compared with the similar samples obtained form powders prepared from nitrates.

This behavior could be correlated with the presence of the intra-granular porosity of the powders prepared from acetates. In this case, during the sintering process a competition between samples' sintering and pores collapse occurred. The lower density in this case could be assigned to the presence of a residual intra-granular porosity that could not be completely eliminated during the sintering process.

3.3.2. Structural characterization

The structure of the sintered powders, as determined by XRD, is presented in Fig. 3 in comparison with the similar XRD patterns of the initial powders thermally treated at 600 °C.

One may notice that the same crystalline phase is present in the sintered ceramics as in the initial powders, but the intensity of the diffraction lines is higher. No secondary phases occurred

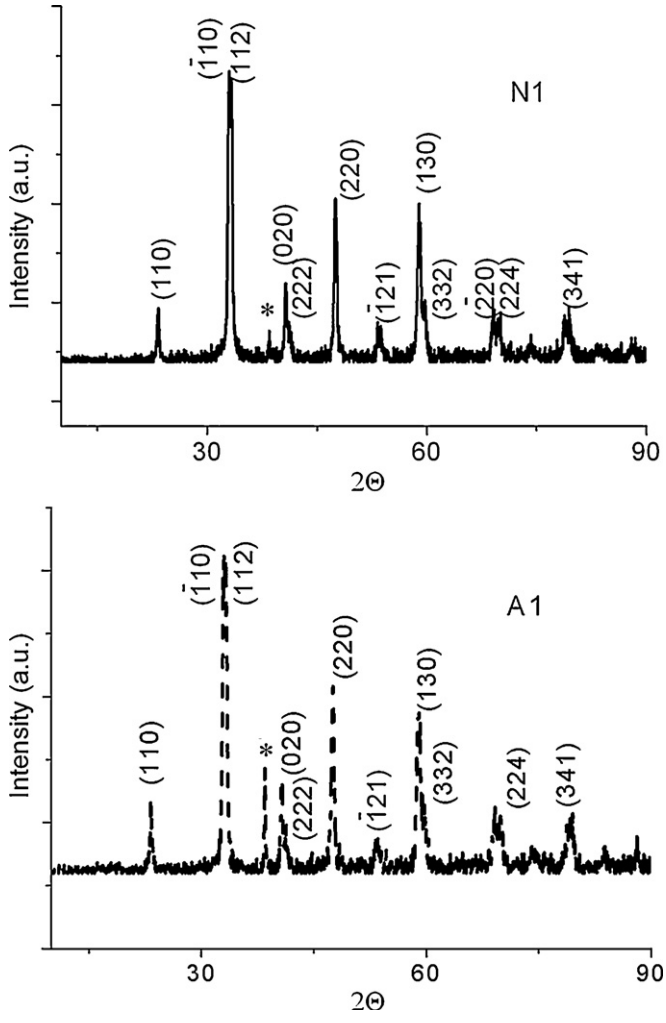

Fig. 1. XRD patterns of the $LaCoO_3$ powder, thermally treated at 600 °C, for 6 h (* – holder).

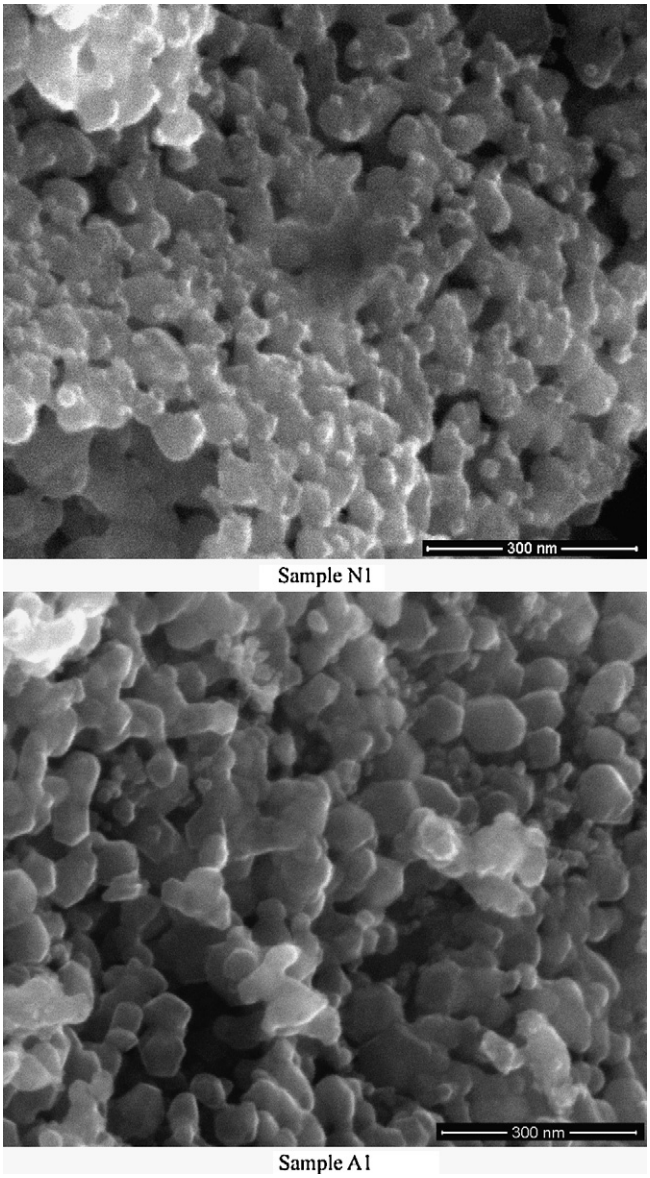

Fig. 2. SEM images of the N1 and A1 powders thermally treated at 600 °C.

Table 1
Crystallographic parameters – (lattice parameters a and c), particle size (D), internal strain (S) – and BET specific surface area of the thermally treated powders at 600 °C.

Sample	a (Å)	c (Å)	c/a	V (Å^3)	$10^{+3} \times S$	D (Å)	BET surf. area (m^2/g)
$LaCoO_3$ (N1)	5.4390(68)	13.1616(226)	2.4199	337.2(1.4)	0.87(25)	537(154)	8.82
$LaCoO_3$ (A1)	5.4455(80)	13.2098(258)	2.4258	339.2(1.7)	1.04(23)	777(217)	13.30

during the sintering process in the sample prepared starting with nitrates. Small amount of Co_3O_4 is identified in the sintered samples prepared starting with acetates.

In Table 3 the value of microstructural factors and lattice constants of the sintered ceramics are presented. These values were obtained using a computerized analysis of the XRD spectra with a proper program X-RAY 3.0 [18].

One may notice that in the case of the sintered samples some differences in the crystallographic parameters occurred depending of the precursors type. Significant differences

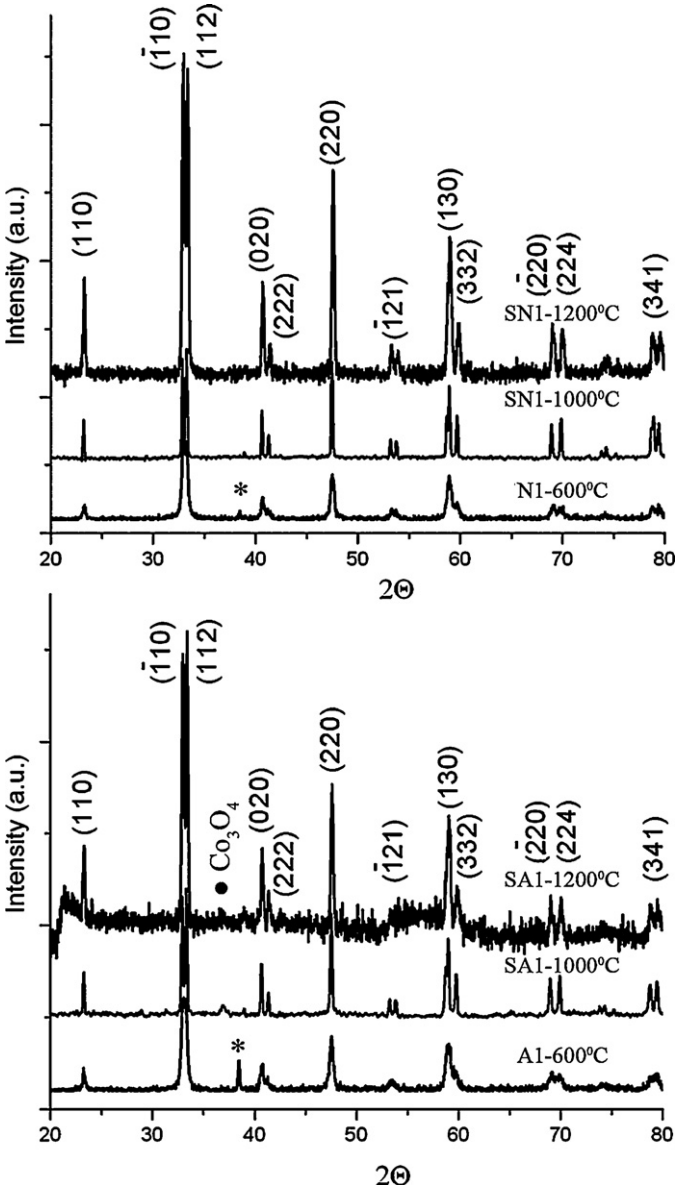

Fig. 3. XRD patterns of the $LaCoO_3$ powder and sintered pellets at 1000 °C and 1200 °C prepared with acetates (* – holder, ● – Co_3O_4).

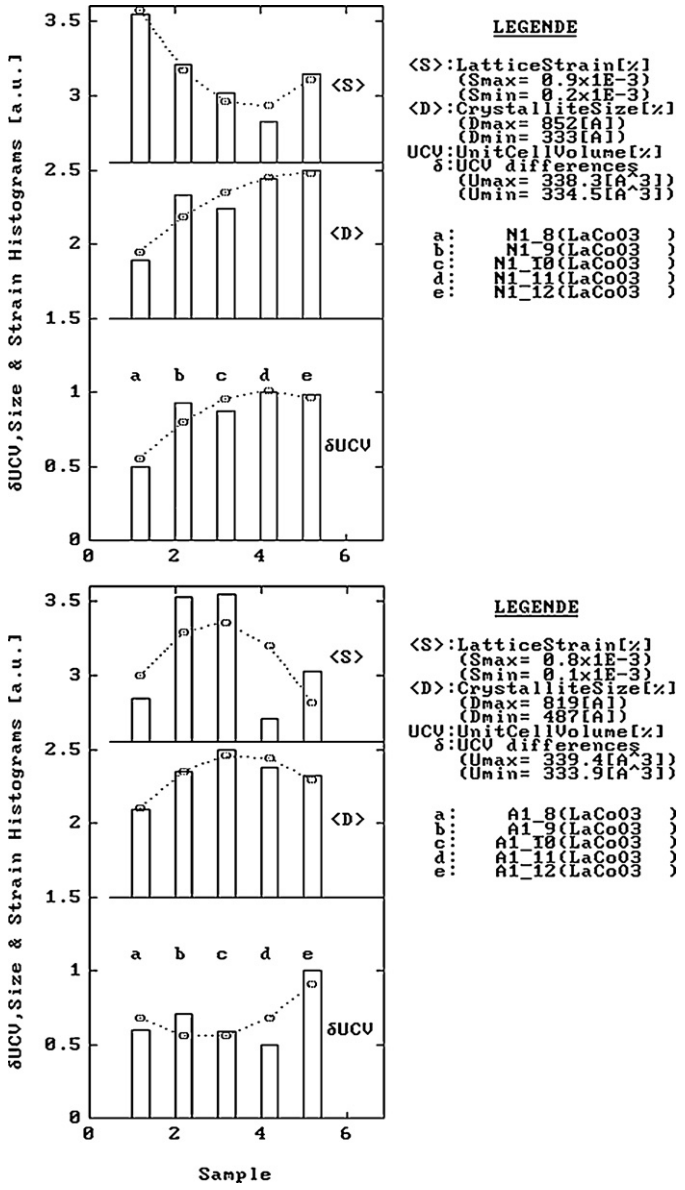

Fig. 4. Microstructural modification depending on thermal treatment and preparation route. (Top) $LaCoO_3$ obtained by nitrate route, (bottom) $LaCoO_3$ obtain by acetate route (In the figures, δUCV reprezents the UCV variation, raported to the highest value a = 800 °C; b = 900 °C, c = 1000 °C; d = 1100 °C; e = 1200 °C).

Table 2
Ceramic properties of the sintered samples at different temperatures.

Sintering temp. (°C)	Shrinkage Δl/l (%)	Open porosity (%)	Experim. density (g/cm^3)	Relative density (%)
Sintered samples from powders obtained from nitrates				
800	1.65	7.12	4.92	67
900	6.00	5.29	6.36	87
1000	10.60	4.77	6.41	88
1100	15.50	1.29	6.50	90
1200	18.85	0.12	6.95	95
Sintered samples from powders obtained form acetates				
800	6.90	6.09	3.90	54
900	10.45	9.36	5.68	77
1000	13.00	5.68	5.71	78
1100	19.25	2.58	5.81	80
1200	24.30	1.31	6.45	88

occurred in the case of the internal lattice strain (*S*) and of the average crystallite size (*D*) (Fig. 4).

For the samples obtained by nitrate route, the evolution of the lattice strain (*S*) and of the average crystallite size (*D*), with the temperature of thermal treatment corresponds to the theoretical expected one. In the case of an ideal lattice when the *S* value decreases the *D* value must increase.

For the acetate route the evolution with the temperature of the average lattice strain (*S*) has a similar trend as the average crystallite size (*D*) variation (Fig. 4). In this case the both *S* and *D* factors behave differently to the theoretically excepted one. The different behavior could be correlated to the formation of Co_3O_4 secondary phase. Its formation could determine the unusual behavior of the *S* and *D* factors with the temperature of thermal treatment. In the same time, due to the presence of the inter-granular pores in this sample, the competition between crystal growth and collapse of the pores could be also taken in to consideration as an explanation of the unusual behavior of the *S* and *D* factors.

The systematic errors of the lattice constants that increase with temperature could be correlated with the presence of the non-stoichiometry.

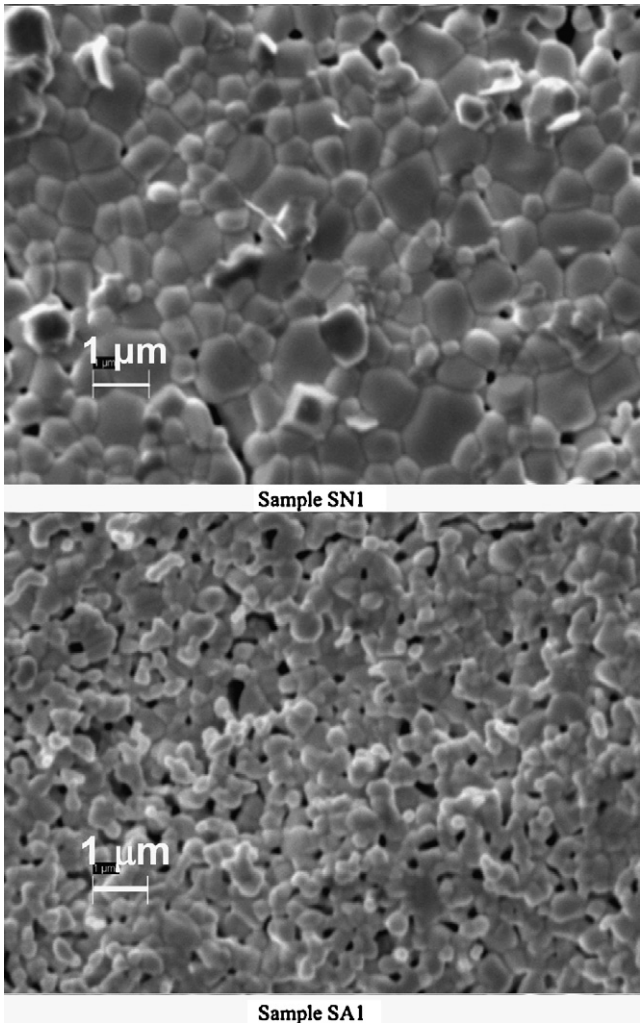

Fig. 5. SEM images of the samples sintered at 1000 °C.

3.3.3. Morphological characterization

The SEM images of the sintered ceramics at 1000 °C, 1100 °C and 1200 °C are presented in Figs. 5–7.

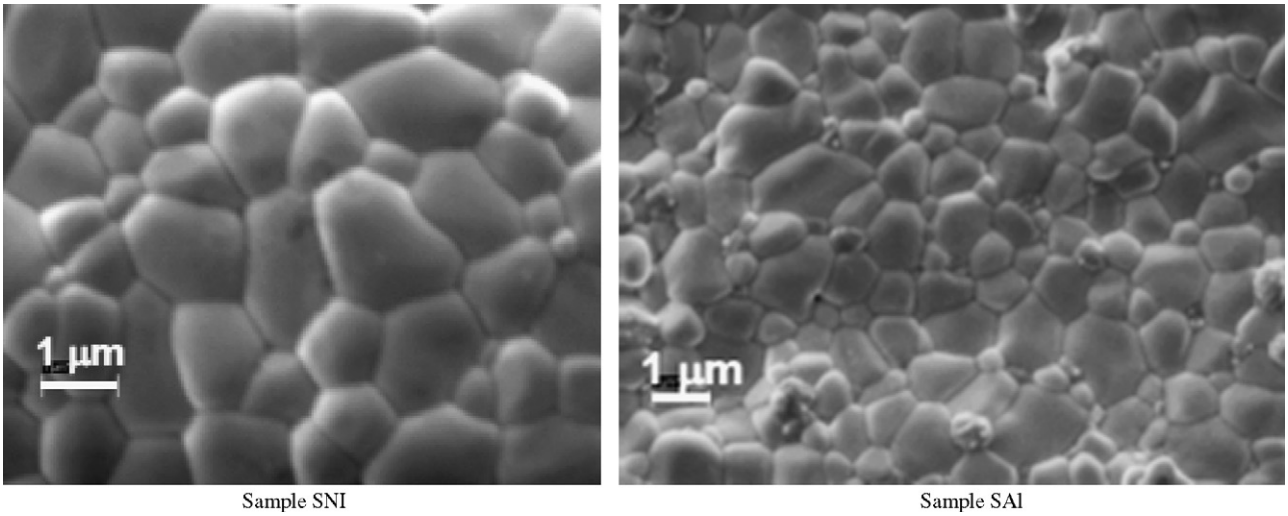

Sample SNI Sample SAl

Fig. 6. SEM images of the samples sintered at 1100 °C.

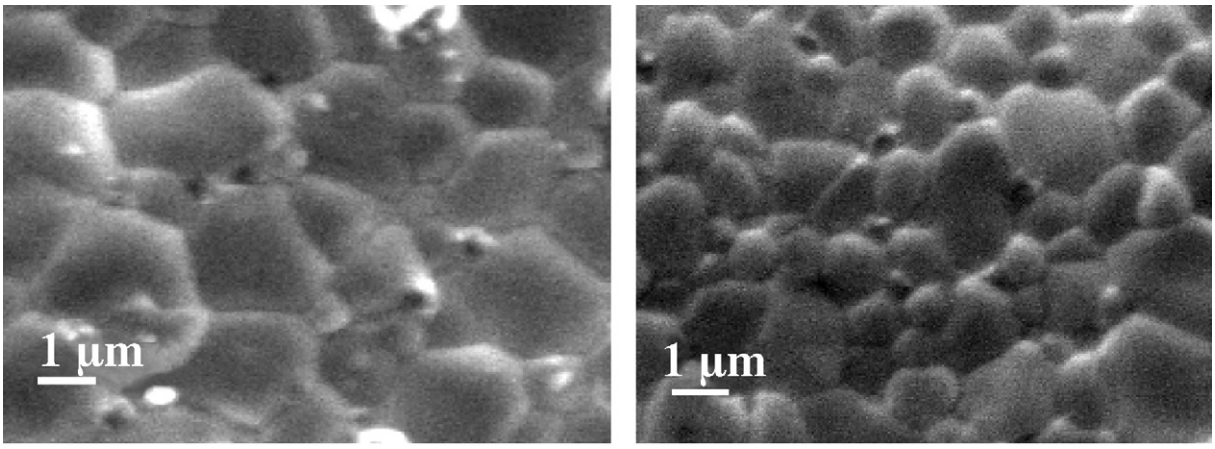

Fig. 7. SEM images of the samples sintered at 1200 °C.

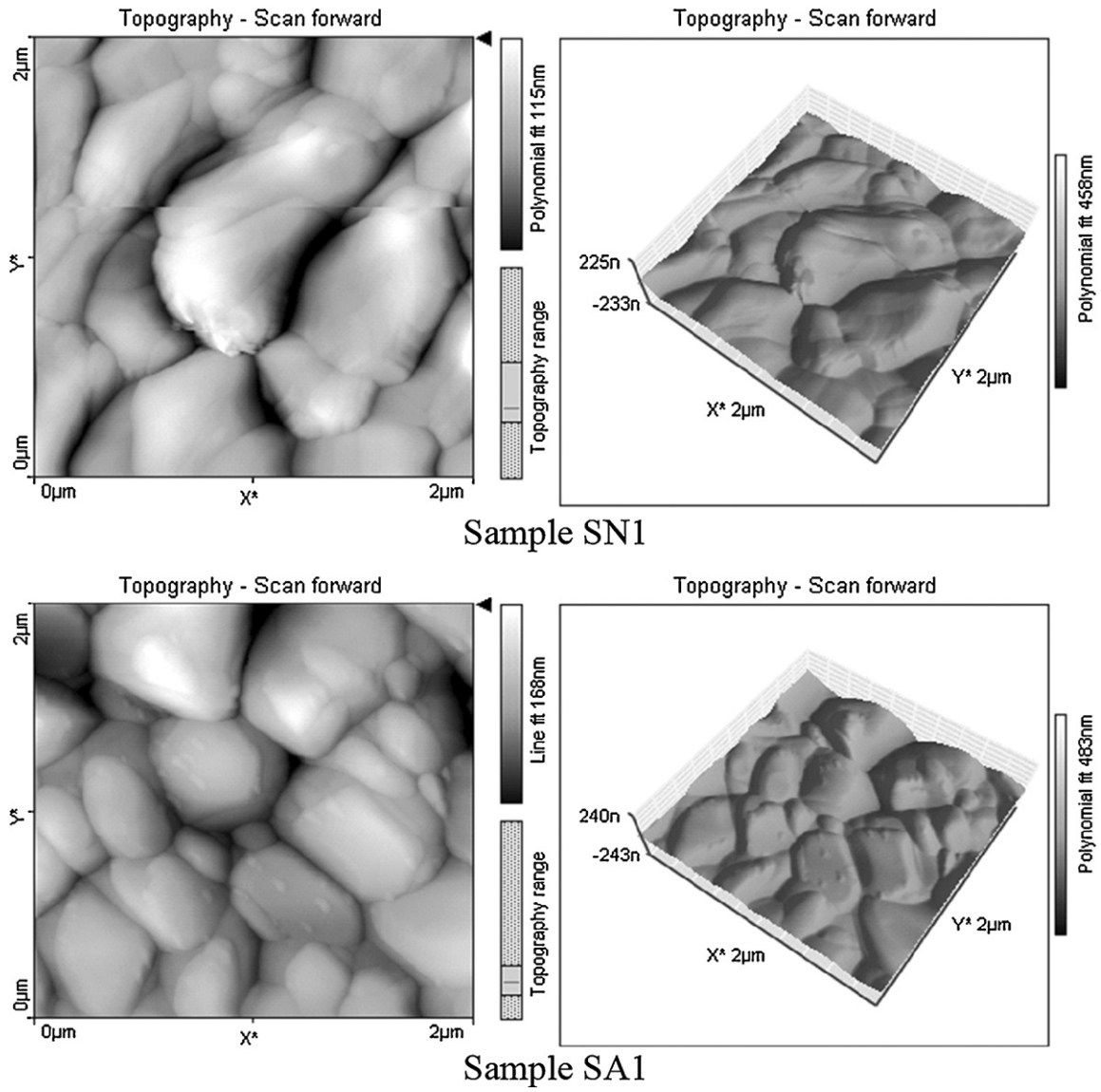

Fig. 8. AFM images of the samples sintered at 1000 °C. (Sample SN1, RMS = 21.21 nm; Sample SA1, RMS = 29.80.)

Table 3
Crystallographic parameters, particle size and internal strain of the sintered powders at different temperatures.

Sample	Temperature (°C)	a (Å)	c (Å)	c/a	V (Å^3)	$10^{+3} \times S$	D (Å)
$LaCoO_3$ (N1)	800	5.43(14)	13.07(46)	2.40	334.50(29)	0.89(12)	333(16)
	900	5.43(48)	13.22(130)	2.43	337.75(93)	0.59(7)	708(44)
	1000	5.43(51)	13.20(155)	2.43	337.3(1.0)	0.42(4)	628(24)
	1100	5.43(53)	13.23(122)	2.43	338.26(97)	0.25(7)	802(51)
	1200	5.43(49)	13.22(132)	2.43	338.14(95)	0.54(7)	852(60)
$LaCoO_3$ (A1)	800	5.43(12)	13.08(40)	2.40	335.02(25)	0.23(27)	487(33)
	900	5.44(4)	13.09(15)	2.40	336.19(9)	0.75(15)	698(95)
	1000	5.44(14)	13.06(56)	2.40	334.90(31)	0.76(6)	819(50)
	1100	5.43(20)	13.05(83)	2.40	333.90(46)	0.12(28)	717(47)
	1200	5.44(60)	13.23(160)	2.43	339.4(1.2)	0.37(6)	674(35)

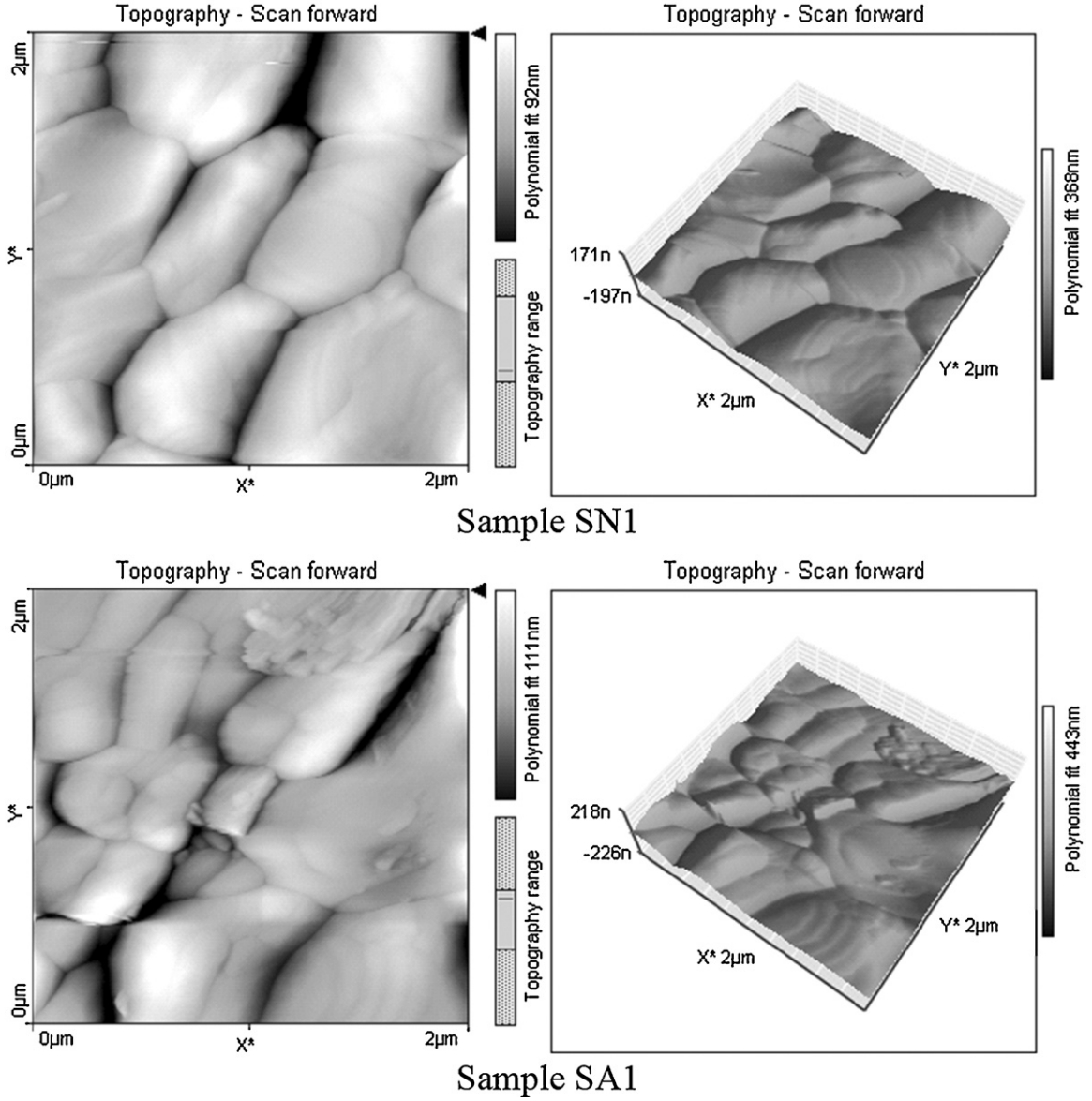

Fig. 9. AFM images of the samples sintered at 1100 °C. (Sample SN1, RMS = 18.81 nm; Sample SA1, RMS = 18.28.)

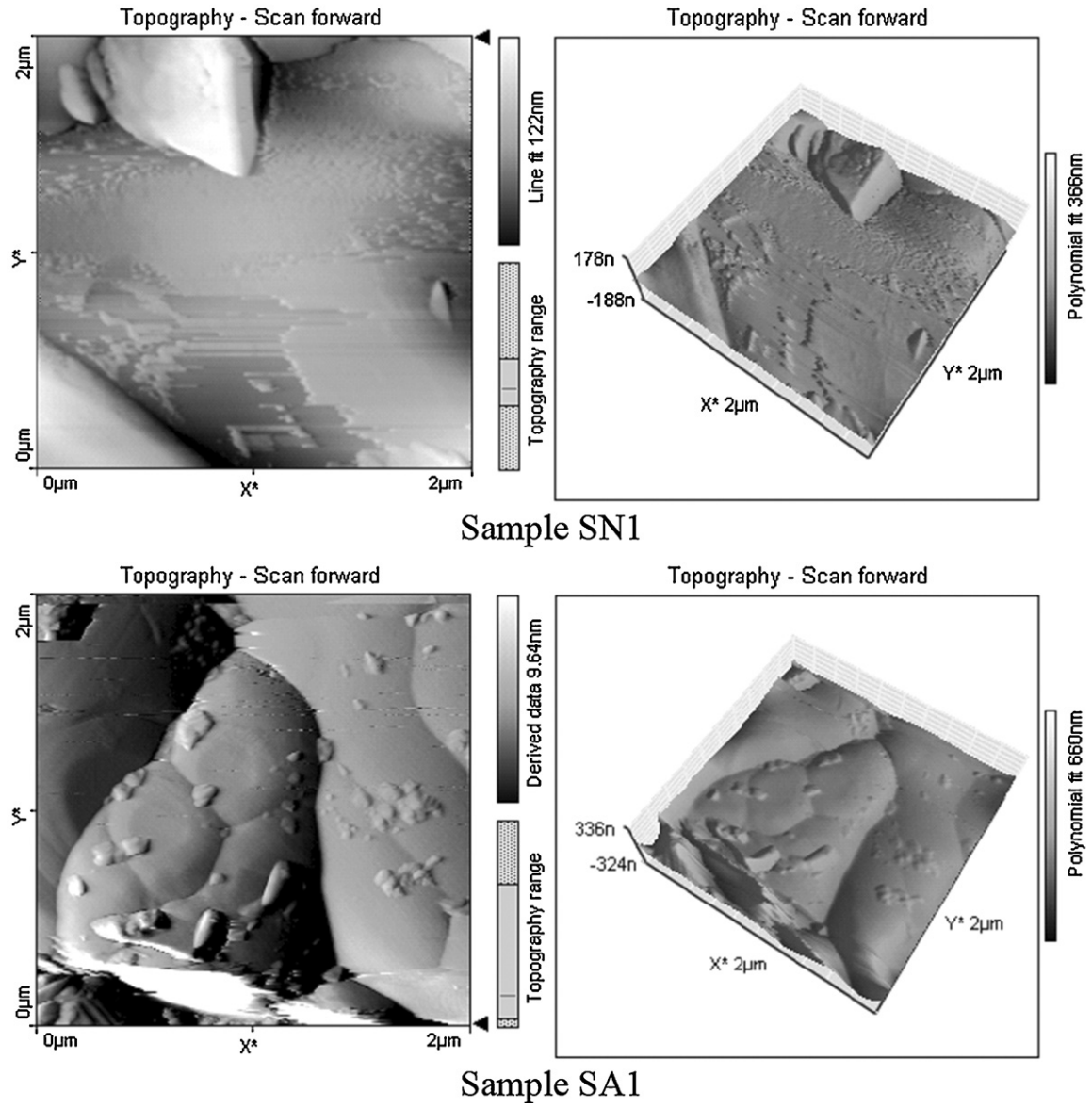

Fig. 10. AFM images of the samples sintered at 1200 °C. (Sample SN1, RMS = 11.21 nm; Sample SA1, RMS = 28.63.)

The SEM images have shown a lower tendency for sintering and a less homogeneous morphology for the ceramics prepared from powders obtained from acetates.

The difference in the sintering properties of the two types of powders is correlated with their different morphology, namely the higher surface area of the powders obtained starting with acetates and the presence of an intra-granular porosity in this later case.

The lower dimension of the particles size observed in the case of the sintered samples obtained from powders prepared starting with acetates could be correlated to the competition that occurs between the collapse of the pores and the particles growth.

The ceramics sintered at 1100 °C from powders obtained from nitrates present uniform grains size distribution and practically no open porosity.

The AFM images measured on the sintered ceramics (in form of pellets) at 1000 °C, 1100 °C and 1200 °C are presented in Figs. 8–10, at a scale of 2 μm × 2 μm, in both bi- and tri-dimensional topographic view. In order to remove unwanted artifacts as tilt and bow, or occasionally noise, the images were corrected by a 2nd order polynomial plane fit (systematically preserved for the 3D representation). Further on, root mean square (RMS) roughness values were calculated and reported for each sample, according to the formula:

$$\mathrm{RMS} = \sqrt{\frac{1}{MN}\sum_{k=0}^{M-1}\sum_{l=0}^{N-1}\left(z(x_k, y_l)\right)^2}$$

The AFM studies are in agreement with the results obtained at larger scale from SEM analysis. As could be seen, the grains are not well separated, without clear grain boundaries, but show locally compact distribution. An

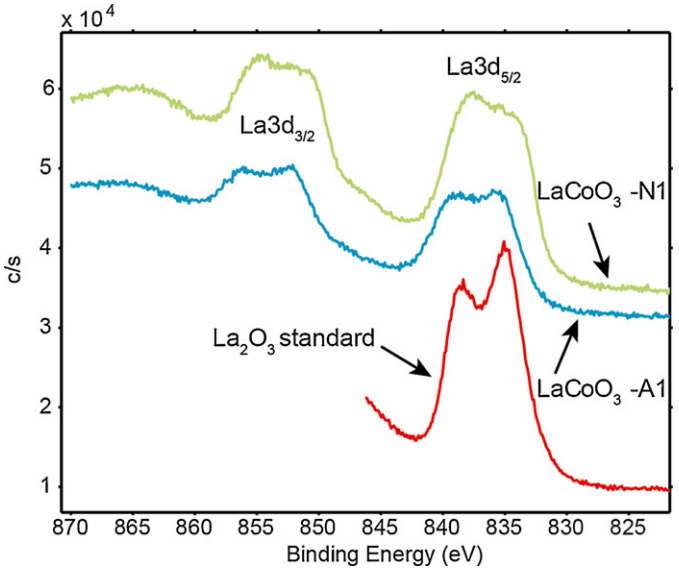

Fig. 11. XPS spectra of La 3d of the samples sintered at 1100 °C.

increase of the grains dimension could be noticed with the increase of the sintering temperature, especially for nitrates-based samples, accompanied by a decrease of the RMS roughness. Note that at 1200 °C the surface morphology is altered, as seen both in SEM and AFM images. Clear separated small particles are visible on top of both SN1 and SA1 samples – Fig. 10, suggesting that at 1200 °C, segregation phenomena may occur (in the bulk of the particles followed by inter-granular transport) due to an enhanced diffusion rate. Regarding the chemical nature of these small grains, located on top of larger particles and in the inter-granular area as well, it may be related to the chemical oxidation state of Co in the superficial region (e.g. small particles of Co_3O_4), as seen in XRD and XPS.

3.4. XPS results

Fig. 11 shows the superimposed XPS spectra of La 3d in the A1, N1 samples calcined at 1100 °C and the La_2O_3 standard. The La 3d core level spectra is dominated by multi electron processes leading to a double peak for each spin–orbit component (3d5/2, 3d3/2)[19]. This structure has been explained by an interatomic charge transfer from the ligand O 2p orbital to the empty La 4f* level occurring in parallel with the creation of the La 3d core hole (shake-up process) or by a strong final state mixing electronic configuration [19,20].

The flattened shape of the 3d band-like spectra for the samples A1, N1 reveals the particular density of states (DoS) in the valence band of the (La, Co) mixed oxides compared with that of the standard La_2O_3 and/or the changes in the degree of covalency bonds of metal-oxygen.

Fig. 12 exhibits the deconvoluted XPS spectra for Co 2p in A1, N1 samples calcined at 1100 °C.

The peak positions (779.7 eV, 795.0 eV respectively) and the presence of the characteristic satellites (789.3 eV, 803.5 eV respectively) for the sample A1 (Fig. 12a) suggest the presence of the Co_3O_4 [21,22] while for the sample N1 (Fig. 12b) could be attributed to Co^{2+} [23].

3.5. Electrical properties

The temperature dependence of the total conductivities of the A1 and N1 samples calcined at 1100 °C is shown in Fig. 13. At this temperature the samples are already single phase and well sinterized.

At low temperature the total conductivity of the A1 and N1 samples is predominantly electronic. In this temperatures range the conductivity of A1 sample is higher than that of N1 sample. For oxides with high electronic conductivity when the porosity is low [24,25] the grain boundaries have negligible effect on the electronic transport. Therefore, the higher conductivity of the

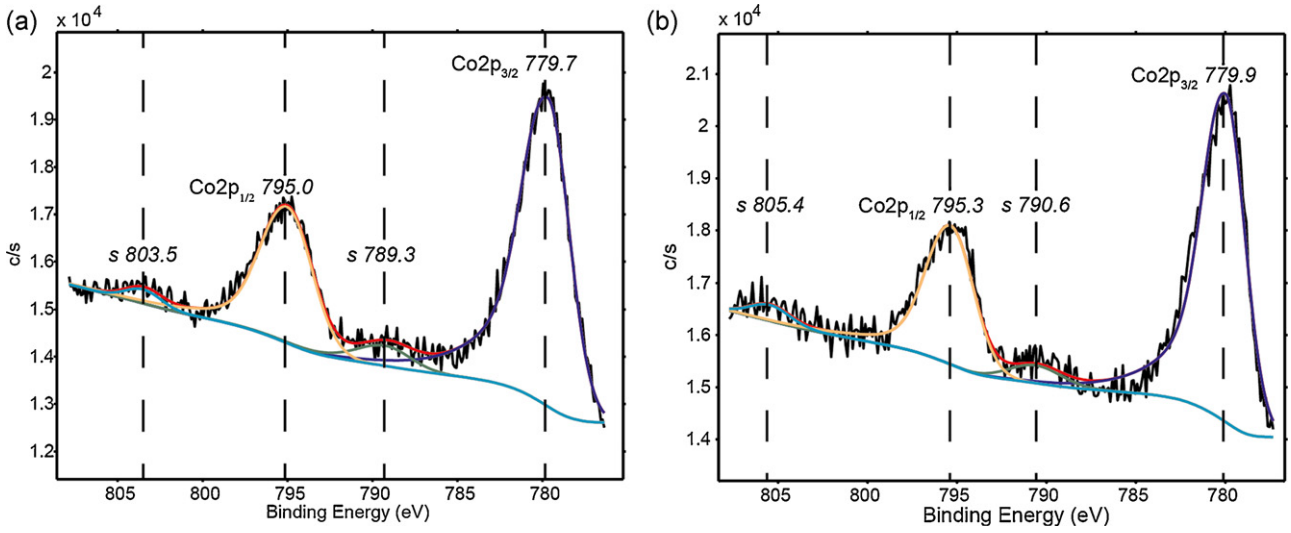

Fig. 12. XPS spectra for Co 2p of the samples sintered at 1100 °C.

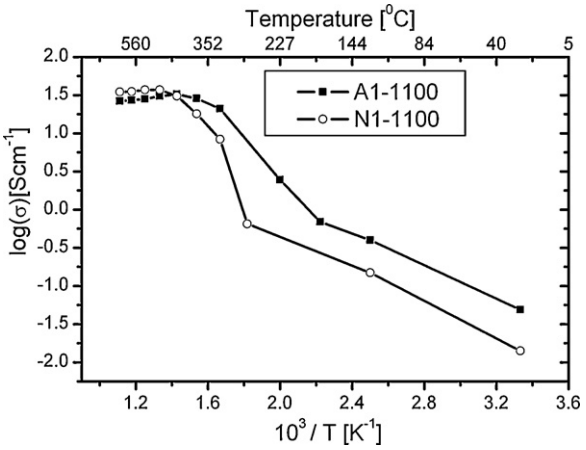

Fig. 13. Arrhenius plot of the total conductivity σ of A1 and N1 calcinated at 1100 °C. The top axis shows the temperatures in °C.

A1 sample at low temperature could be explained by the presence of Co_3O_4 on its surface.

With increasing the temperature it can be seen that the total conductivity of the samples is increasing and above 400 °C the values of conductivity for N1 samples are slight higher than for A1 sample. This is an indication that at high temperatures the ionic conductivity of the N1 sample is greater than the ionic conductivity of the A1 sample. This behavior may be explained by higher average grain size of N1 sample (Figs. 5 and 8) which lowers grain boundaries resistance to the ionic transport. The conductivity values at low and high temperature were in good agreement with previously published data [13,26,27].

4. Conclusions

Sintering studies of $LaCoO_3$ powders prepared by sol–gel method using two types of precursors, nitrates or acetates and citric acid as chelating agent were done.

Pure $LaCoO_3$, perovskite nano-powders were obtained at 600 °C, for both precursors, that represents a low temperature as compared to the data mentioned in the literature.

Dense ceramics could be obtained from both synthesized powders in the 1000–1200 °C temperature range.

The sintered samples were characterized by SEM, XRD, AFM and XPS.

The best results in our study have been obtained using $LaCoO_3$ powders obtained form nitrates, sintered at 1100 °C.

The electrical proprieties of the samples were investigated by impedance spectroscopy. The higher electronic conductivity of ceramics obtained from powder based on acetates at low temperature could be explained by the presence of Co_3O_4 on its surface.

Acknowledgements

This contribution was carried out within the Research Program 7, Physical Chemistry of Oxide Materials of the ''Ilie Murgulescu'' Institute of Physical Chemistry and the frame of inter-academic collaboration with Jozef Stefan Institute, Ljubljana, Slovenia supported by the Romanian Academy. The author Rareş Scurtu acknowledges the support of CNCSIS-UNIFISCU project number PNII-RU 196/2010.

References

[1] C. Matei, D. Berger, P. Marote, S. Stoleriu, J. Deloume, Lanthanum-based perovskites obtained in molten nitrates or nitrites, Progress in Solid State Chemistry 35 (2007) 203–209.
[2] D. Berger, N. Van Landschoot, C. Ionica, F. Papa, V. Fruth, Synthesis of pure and doped lanthanum cobaltite by the combustion method, Journal of Optoelectronics and Advanced Materials 5 (2003) 719–724.
[3] K. Kleveland, N. Orlovskaya, T. Grande, A.M.M. Moe, M.A. Einarsrud, K. Breder, G. Gogotsi, Ferroelastic behavior of $LaCoO_3$ based ceramics, Journal of the American Ceramic Society 84 (2001) 2029–2033.
[4] R. Schmidt, J. Wu, C. Leighton, I. Terry, Dielectric response to the low-temperature magnetic defect structure and spin state transition in polycrystalline $LaCoO_3$, Physical Review B 79 (2009) 125105.
[5] F. Li, X. Yu, L. Chen, H. Pan, X. Xin, Solid state synthesis of $LaCoO_3$ perovskite nanocrystals, Journal of the American Ceramic Society 85 (2002) 2177–2180.
[6] S. Faaland, T. Grande, M.A. Einarsrud, P.E. Vullum, R. Holmestad, Stress–strain behavior during compression of polycrystalline $La_{1-x}Ca_xCoO_3$ ceramics, Journal of the American Ceramic Society 88 (2005) 726–730.
[7] M. Popa, M. Kakihana, Synthesis of lanthanum cobaltite ($LaCoO_3$) by the polymerizable complex route, Solid State Ionics 151 (2002) 251–257.
[8] M. Popa, J.M. Calderon-Moreno, Lanthanum cobaltite nanoparticles using the polymeric precursor method, Journal of the European Ceramic Society 29 (2009) 2281–2287.
[9] E. Campagnoli, A. Tavares, L. Fabbrini, I. Rossetti, Y.A. Dubitsky, A. Zaopo, L. Forni, Effect of preparation method on activity and stability of $LaMnO_3$ and $LaCoO_3$ catalysts for the flameless combustion of methane, Applied Catalysis B 55 (2005) 133–139.
[10] H. Taguchi, S. Yamada, M. Nagao, Y. Ichikawa, K. Tabata, Surface characterization of $LaCoO_3$ synthesized using citric acid, Materials Research Bulletin 37 (2002) 69–76.
[11] H. Hwang, A. Towata, M. Awano, K. Maeda, Sol–gel route to perovskite-type Sr-substituted $LaCoO_3$ thin films and effects of polyethylene glycol on microstructure evolution, Scripta Materialia 44 (2001) 2173–2177.
[12] J. Guo, H. Lou, Y. Zhu, X. Zheng, La-based perovskite precursors preparation and its catalytic activity for CO_2 reforming of CH_4, Materials Letters 57 (2003) 4450–4455.
[13] S. Nakayama, M. Okazaki, Y.L. Aung, M. Sakamoto, Preparations of perovskite-type oxides $LaCoO_3$ from three different methods and their evaluation by homogeneity, sinterability and conductivity, Solid State Ionics 158 (2003) 133–139.
[14] X. Chang, C. Zhang, X. Dong, W. Zhou, W. Jin, Z. Shao, N. Xu, Effects of sintering atmospheres on sintering behavior, electrical conductivity and oxygen permeability of mixed-conducting membranes, Journal of Membrane Science 316 (2008) 128–136.
[15] L. Predoana, B. Malic, M. Kosec, M. Carata, M. Caldararu, M. Zaharescu, Characterization of $LaCoO_3$ powders obtained by water-based sol–gel method with citric acid, Journal of the European Ceramic Society 27 (2007) 4407–4411.
[16] D. Johnson, Zview, Scribner Associates, Inc., 2010.
[17] L. Predoana, A. Jitianu, B. Malic, M. Zaharescu, Study of the gelling process in the La–Co–citric acid system, Journal of the American Ceramic Society 95 (2012) 1068–1076.
[18] N. Dragan, D. Crisan, C. Lepadatu, Fast analysis of the XRD profile with the XRAY 3. 0 program, Romanian Journal of Materials 33 (2003) 133–148.
[19] K. Bolwin, W. Schnurnberger, G. Schiller, Influence of valence band states on the core hole screening in lanthanide perovskite compounds, Zeitschrift für Physik B Condensed Matter 72 (1988) 203–209.

[20] M.M. Natile, E. Ugel, C. Maccato, A. Glisenti, $LaCoO_3$: effect of synthesis conditions on properties and reactivity, Applied Catalysis B 72 (2007) 351–362.

[21] J. Dacquin, C. Lancelot, C. Dujardin, P. Da Costa, G. Djega-Mariadassou, P. Beaunier, S. Kaliaguine, S. Vaudreuil, S. Royer, P. Granger, Influence of preparation methods of $LaCoO_3$ on the catalytic performances in the decomposition of N_2O, Applied Catalysis B 91 (2009) 596–604.

[22] J. Villoria, M. Alvarez-Galvan, R. Navarro, Y. Briceño, F. Gordillo Alvarez, F. Rosa, J. Fierro, Zirconia-supported $LaCoO_3$ catalysts for hydrogen production by oxidative reforming of diesel: optimization of preparation conditions, Catalysis Today 138 (2008) 135–140.

[23] J.F. Moulder, J. Chastain, Handbook of X-ray Photoelectron Spectroscopy: A Reference Book of Standard Spectra for Identification and Interpretation of XPS Data, Physical Electronics Division, Perkin-Elmer Corp., 1992.

[24] V.V. Kharton, F.M. Figueiredo, A.V. Kovalevsky, A.P. Viskup, E.N. Naumovich, A.A. Yaremchenko, I.A. Bashmakov, F.M.B. Marques, Processing, microstructure and properties of $LaCoO_3$-[delta] ceramics, Journal of the European Ceramic Society 21 (2001) 2301–2309.

[25] J. Van Roosmalen, J. Huijsmans, L. Plomp, Electrical conductivity in $La_{1-x}Sr_xMnO_3$+[delta], Solid State Ionics 66 (1993) 279–284.

[26] F. Li, J.-F. Li, Effect of Ni substitution on electrical and thermoelectric properties of $LaCoO_3$ ceramics, Ceramics International 37 (2011) 105–110.

[27] S. Uhlenbruck, F. Tietz, High-temperature thermal expansion and conductivity of cobaltites: potentials for adaptation of the thermal expansion to the demands for solid oxide fuel cells, Materials Science and Engineering B 107 (2004) 277–282.